A permanent magnet to search for long-lived $\pi^+\pi^-$ atoms

Received May 25, 2012

S. Aogaki[1],
M. Chiba[2],
Y. Iwashita[3],
M. Kobayashi[4],
K. Okada[1] and F. Takeutchi[1]
[1]Kyoto-Sangyo University,
[2]Tokyo Metropolitan University,
[3]Kyoto University,
[4]KEK

1. Introduction

The DIRAC experiment [1] has been running at CERN PS measuring lifetimes of $\pi^+\pi^-$, $K^+\pi^-$ and π^+K^- atoms by the DIRAC spectrometer as shown in Fig. 1. Up to now more than 21,000 $\pi^+\pi^-$ pairs originated from a breakup of the $\pi^+\pi^-$ atom ($A_{2\pi}$) were identified and the overall accuracy of the $A_{2\pi}$ lifetime is about 9% in accordance with the DIRAC proposal.

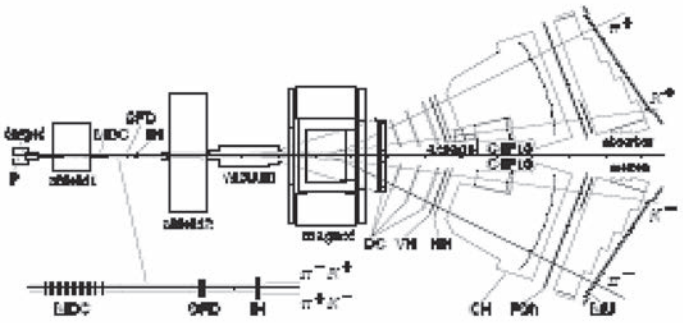

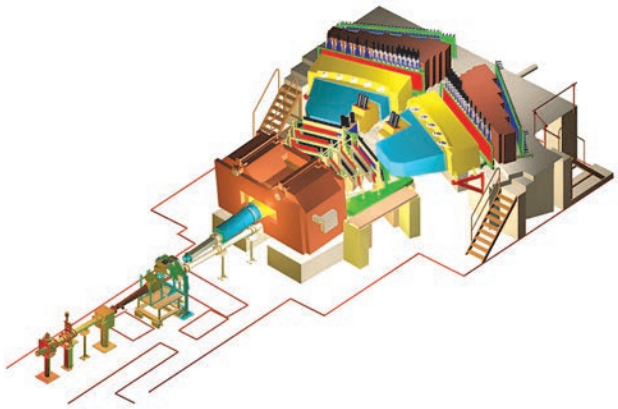

Fig. 1: *DIRAC Spectrometer: Upper: plane view, Lower: perspective view*
[Upstream] MDC: microdrift gas chambers, SFD: scintillating fiber hodoscopes, IH: ionization hodoscope, [Downstream] Magnet: spectrometer magnet with two arms, DC: drift chambers, VH: vertical hodoscope, HH : horizontal hodoscope, CH: Cherenkov detectors containing nitrogen , heavy gas C_4F_{10} and aerogel, PSh: shower detectors, MU: muon detectors .

A new DIRAC proposal [2] was presented to measure long-lived $\pi^+\pi^-$ atoms at CERN PS. This measurement allows to extract the difference of *S*-wave $\pi\pi$-scattering length $|a_0 - a_2|$ with accuracy of 4.3%. In addition, the observation of long-lived (metastable) $A_{2\pi}$ states will be performed with the same setup. The observation opens a possibility to measure the energy difference between *ns* and *np* states and to determine the value of another combination $2a_0 + a_2$ of $\pi\pi$ scattering length in a model-independent way. The measurement of two combinations gives a_0 and a_2 separately. The long-lived $\pi^+\pi^-$ atoms are generated at the Be target and broken up at the Pt foil as shown in Fig. 2. The distance between the Be target and the Pt foil was chosen to be 100 mm to exclude an interaction of the primary beam halo with the Pt foil.

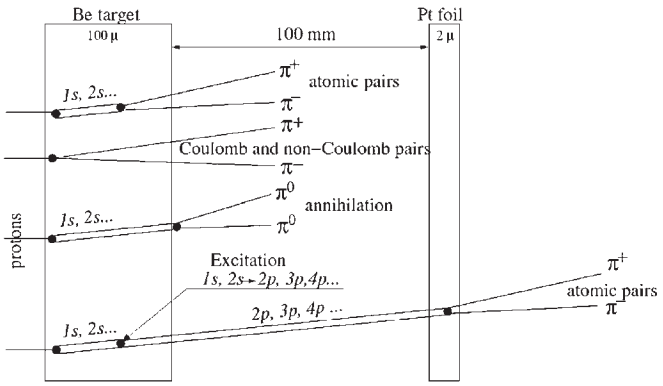

Fig. 2: *The long-lived $\pi^+\pi^-$ atoms are generated at the Be target and broken up at the Pt foil.*

Figure 2 shows that $\pi^+\pi^-$ pairs are produced at several stages of the reaction. They are atomic pairs from long-lived atoms produced in the Platinum foil, atomic pairs from the Beryllium target , Coulomb pairs, "non-Coulomb pairs" and accidentals. Fig. 3 presents a *Y* component of relative momentum *Q* of $\pi^+\pi^-$ pairs. The cuts on $|Q_X| < 1$ MeV/c and $|Q_L| < 1$ MeV/c have been applied. The quantity Q_T, Q_L, Q_X and Q_Y is the transverse, longitudinal, *X* and *Y* components of the relative momentum Q in the atomic pair c.m.s. Simulation shows that in each projection such criterion selects more than 90% of "atomic pairs" from long-lived atoms. Hatched area is a sum of all pairs produced in Beryllium target and light area corresponds to "atomic pairs" from long-lived atoms broken in the Platinum foil.

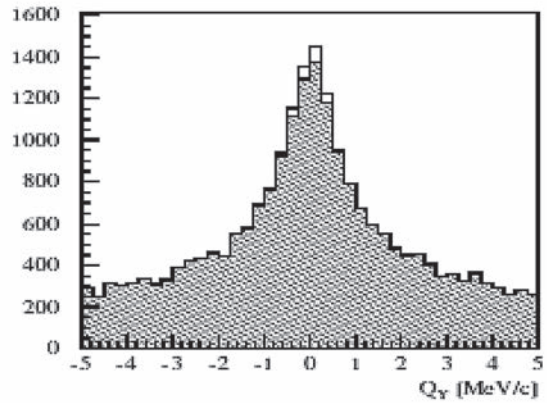

Fig. 3: *Simulated distribution of $\pi^+\pi^-$ pairs over Q_Y with criteria: $|Q_X| < 1$ MeV/c, $|Q_L| < 1$ MeV/c. "Atomic pairs" from long-lived atoms (light area) above background produced in Beryllium target (hatched area)*

The signal-to-background ratio is small. It can be improved by installation of an additional retractable magnet which induces the horizontal magnetic field in the gap between Be target and Pt foil. A magnet with the bending power of 0.01 Tm (Tesla*meter) would shift the Q_Y value by 6 MeV/*c* only for the pairs produced in the Be target leaving unchanged the Q_Y distribution of the pairs produced in the Pt foil. The magnet with such characteristics is installed (see Fig. 4).

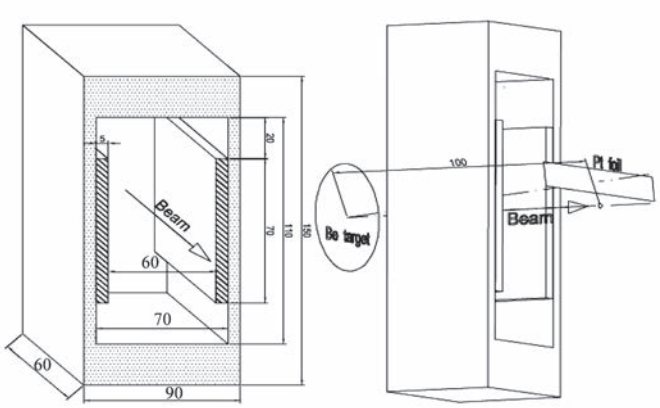

Fig. 4: *Permanent magnet dimensions and arrangement of the Beryllium target, permanent magnet and Platinum foil.*

Fig. 5 shows the resulting Q_Y distribution with the improved signal-to-background ratio. We could discriminate the atomic pairs from the background easier than in Fig. 3.

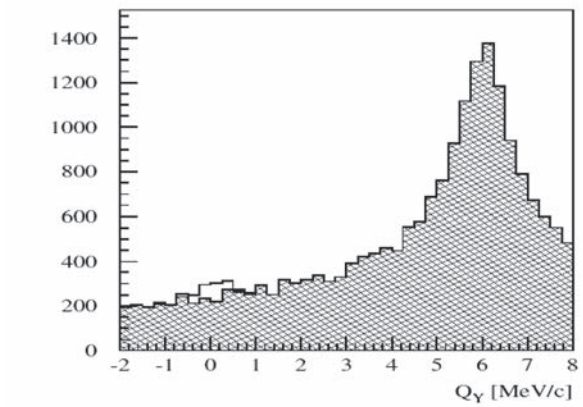

Fig. 5: *Simulated distribution of $\pi^+\pi^-$ pairs over Q_Y with criteria: $|Q_X| < 1$ MeV/c, $|Q_L| < 1$ MeV/c. Additional magnet is implemented. "Atomic pairs" from long-lived atoms (light area) above background produced in Beryllium target (hatched area).*

A new sample of simulated data with the additional magnet has been fitted with the sum of the distributions of atomic pairs from long-lived atoms, "Coulomb pairs" and "non-Coulomb pairs". The atomic pairs produced in the Be target with the Q_Y about 6MeV/c are absent in the fit region.

The fit results for distribution over Q_L (with cut $Q_T < 1$ MeV/c) are presented in Fig. 6.

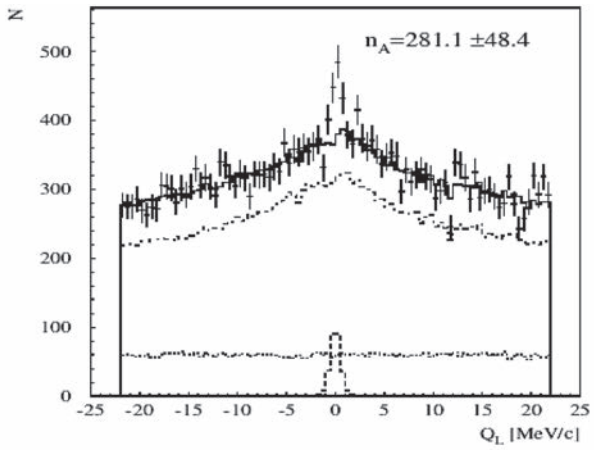

Fig. 6: *Simulated distribution of $\pi^+\pi^-$ pairs over Q_L, with criterion $Q_T < 1$ MeV/c. "Experimental" data (points with error bars) are fitted by a sum of "atomic pairs" from longlived states (dashed line), "Coulomb pairs" (by dotted-dashed line), "non-Coulomb pairs" (dotted line). The background sum is shown by the solid line.*

Number of atomic pairs are found to be:

$$n_A^l = 281 \pm 48 \qquad (1)$$

Analysis of the experimental data accounting widths of the atomic pairs distribution over different components of the relative momentum Q allows to find the variable F which provides the distributionof atomic pairs with the best signal-to-background ratio:

$$F = \sqrt{\left(\frac{Q_X}{0.50}\right)^2 + \left(\frac{Q_Y}{0.32}\right)^2 + \left(\frac{Q_L}{0.56}\right)^2} \qquad (2)$$

Here 0.50, 0.32 and 0.56 in units of Mev/c are RMSs of the atomic pairs distribution over corresponding components of the relative momentum Q.

Fig. 7 presents results of analysis for distribution of $\pi^+\pi^-$ pairs over F. We find excess events of the atomic pairs over the solid line at $F < 3$ MeV/c. It provides a greater number of found atomic pairs due to the weaker cut on $Q_T < 2$ MeV/c and a better signal-to-error ratio:

$$n_A^l = 327 \pm 37 \qquad (3)$$

$$\frac{n_A}{\delta n_A} = 8.8 \qquad (4)$$

It is worth noting that the simulated number $\boldsymbol{n}_A^l$ is 310.

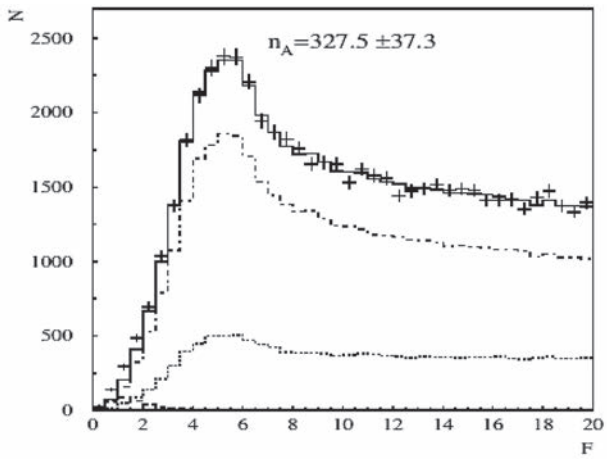

Fig. 7: *Simulated distribution of $\pi^+\pi^-$ pairs over F, with criterion $Q_T < 2$ MeV/c. "Experimental" data (points with error bars) are fitted by a sum of "atomic pairs" from long-lived states (dashed line), "Coulomb pairs" (by dotted-dashed line), "non-Coulomb pairs" (dotted line). The background sum is shown by the solid line.*

In order to declare an observation of long-lived $\pi^+\pi^-$ atoms it is needed to achieve a ratio between signal and error greater than 5. The current simulation provides the ratio of 8.8. This means that probability to observe long-lived $\pi^+\pi^-$ atoms is close to 100%. In the approach without the additional permanent magnet the accuracy of effect separation will be worse. At equal conditions the simulated number of reconstructed atomic pairs is

$$n_A^l = 334 \pm 89 \qquad (5)$$

To achieve the value of 5 in the signal-to-error ratio, required for the observation, the needed statistic should be increased by 1.8 that can be accomplished with a high efficiency of the event reconstruction and/or a longer run time.

2. Permanent magnet

We had experienced to fabricate a small analyzing magnet consist of neodymium [3] to get better separation of π^+ and π^- tracks broken from an $\pi^+\pi^-$ atom in scintillation fiber detectors [4] set between the production target and the main analyzing magnet in the Dirac spectrometer [5]. We utilized a permanent magnet to realize the required-measuring conditions. The magnet should be installed in the vacuum target station just after the production target made of Beryllium in Fig. 1 where the primary-proton beam delivered from CERN PS passing through. The beam with the halos should pass through without hit the magnet. The magnet is set between the production target

and the Platinum foil where the atomic pairs are broken as in Fig.4. The distance is determined to be 10cm so that most of the long-lived atomic pairs are alive. The magnetic field strength should not much higher than 0.1T not to quench the *p* or *d* states of the atoms to the s state since the quench effect is proportional to the square of the field strength. The bending power of BL of 0.01 Tm is strong enough to move aside the peak of the short-lived $\pi^+\pi^-$ pairs in Q_Y as shown in Fig. 5. At and after the breaking target the magnetic field should be low enough not to bend the charged pions broken from $\pi^+\pi^-$ atoms.

We utilize a permanent magnet to realize the required conditions. Permanent magnet has advantages over electromagnets. It does not need an electric current to magnetize which generates heat in the vacuum setting. The magnetic field is stable since there is no thermal and mechanical change due to the electric current. But it is reported that the magnetic field strength would decrease due to strong irradiations from protons and neutrons, on the other hand the degradation seems rather weak for gamma rays [6 - 8]. We should keep a watch on it in the radiation environment.

We made a permanent magnet as shown in Figs.8 and 9. A couple of neodymium pieces of 70x60 mm^2 with the thickness of 5 mm were employed. The gap is 60 mm and the integrated magnetic field along the beam is around 0.01 Tm. The external sizes of the magnet are 150 mm wide, 90 mm high and 60 mm deep. Two permanent magnet poles are glued on the inner facing surfaces of the iron frame. Each permanent magnet is composed of a piece of 70 mm x 40 mm, two pieces of 30 mm x 20 mm, and a piece of 20 mm x 10 mm, as shown in Fig. 9. The permanent magnet material of the largest plates is N35 and that of the rest is N40, where the remanent field Br of N40 and N35 are specified as 1.22~1.25T and 1.17~1.22 T, respectively. The leg thickness of the iron frame is 20mm and the thickness of the top and bottom plate is 10mm. The iron frame is made of structural mild steel, which should correspond to SS 400. Because the magnetic field in the gap is not generated by the iron part but the permanent magnets, the field should not be much affected by the difference of irons, as long as it has enough high permeability.

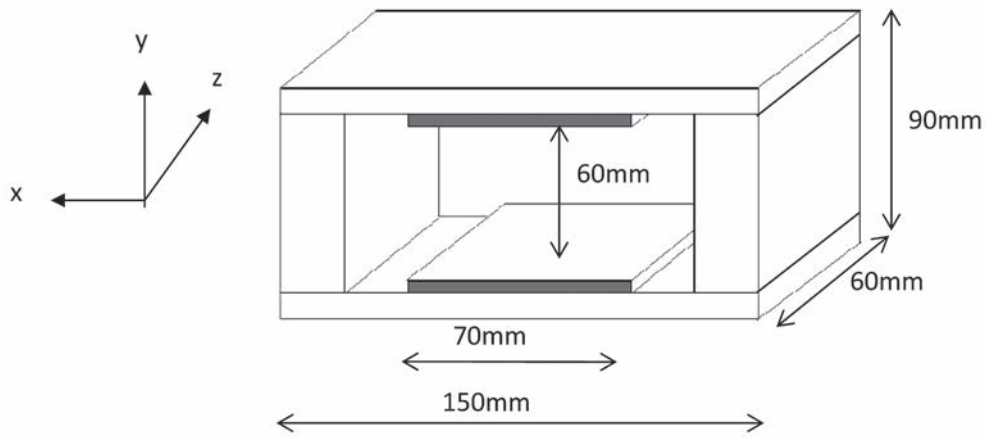

Fig. 8: *A drawing of the permanent magnet with the axes of the coordinates*

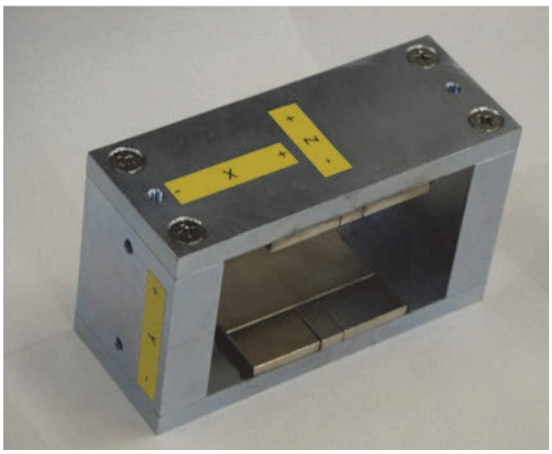

Fig. 9: *A picture of the permanent magnet. The directions of + and - for the X coordinate labeled on the surface should be reversed. The right-handed coordinate system is employed as shown in Fig. 8.*

3. Magnetic field simulation

RADIA version 4.29[9-11] is used for the magnetic field calculation. The calculated geometry is shown in Fig. 10, where the permanent magnet plate dimensions are 5mm in thickness, 60mm in length and 70mm in width. The coordinate system is shown in the figure, where the origin coincides with the centroid of the magnet. In the calculation, three symmetries are used: x-y plane, y-z plane, and z-x plane, which reduces the system 1/8 comparing with the full system. The remanent flux density of the magnet is assumed to be 1.22T and the recoil permeability of 1.05. The return yoke material is "steel37" equipped in RADIA, which is an inexpensive steel with C<0.13%.

Figure 11 shows the y-component of the magnetic flux density along z on x=y=0 line and x=y=10. The integrated values on these lines are as follows:

$$\int_{0mm}^{100mm} By_{x=0,y=0}(z)\,dz = 0.00490\,[\mathrm{T.m}], \quad \int_{0mm}^{100mm} By_{x=10,y=10}(z)\,dz = 0.00492\,[\mathrm{T.m}], \tag{6}$$

where only the half of the region is counted along the path. The x-component and y-component along x=y=10mm line are shown in Fig. 12,

$$\int_{0mm}^{100mm} Bx_{x=10,y=10}(z)\,dz = 0.316\,[\mathrm{mT.m}], \quad \int_{0mm}^{100mm} Bz_{x=10,y=10}(z)\,dz = 1.297\,[\mathrm{mT.m}]. \tag{7}$$

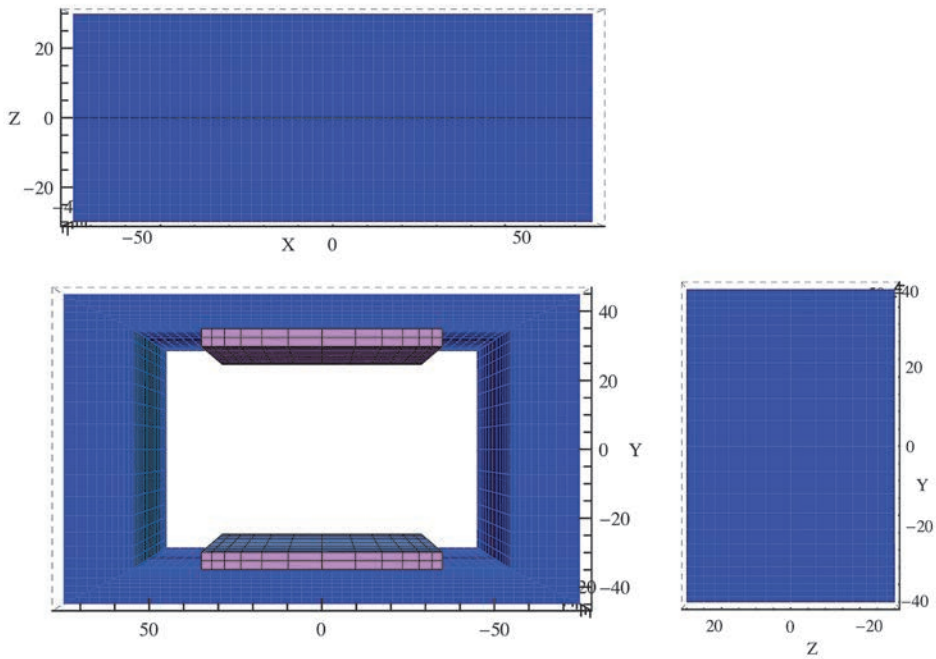

Fig. 10: *Calculated geometry, the unit is in mm: Top View, Front view and side view.*

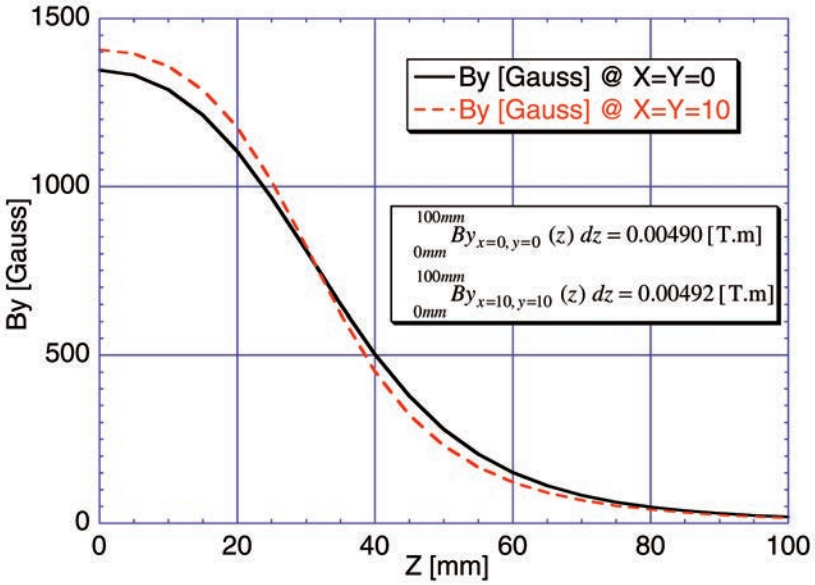

Fig. 11: *Calculated By distributions on lines of x=y=0 and x=y=10mm.*

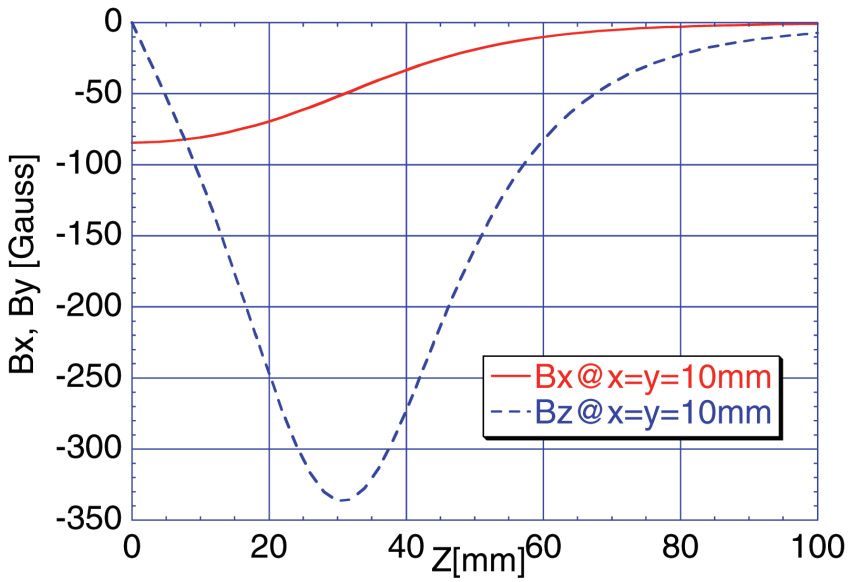

Fig. 12: *Calculated Bx and Bz distributions on line x=y=10mm.*

4. Magnetic field measurement

In this measurement we used 3MH3: 3-Axis Digital Tesla-meter [12]. This Tesla-meter has a three-axis Hall probe, which is fixed on an x-y stage. The probe head has 4 mm width, 2 mm thickness, and 15 mm length. The field sensitive area is 0.15 mm x 0.01 mm x 0.15 mm. The measurement range along *z*-axis is from -100 mm to 100 mm with 4 mm steps. *X* and *Y*-coordinates of the measurement lines are from -6 mm to 6 mm with 2 mm steps. We also measured additional points on four lines of (x, y) = {(-10, -10), (-10, 10), (10, -10), (10, 10)}. The alignment error on the magnet against the x-y stage axis is less than 0.1mm.

The measured magnetic field is calibrated using a NMR probe. And in this measurement, the room temperature changed from 19.0 to 19.3 ℃. The values are also calibrated using with temperature coefficient (TC). A TC of the probe is $1*10^{-3}$/℃. These BL values are calculated by Simpson's formula. Figure 13 shows the y-component of the magnetic flux density along *z*-axis on x = y = 0 and x = y = 10. Figure 14 shows the same information as Fig. 13 on x = y = 10 and x = y = -10. Figure 15 and 16 show the x and y component of the magnetic flux density along *z*-axis on x = y = 0 and x = y = 10, respectively.

The calculated data of Bz has 0 value at z = 0. Differences of BL values are also calculated. The results of these are shown in Table 1.

The positioning angle accuracy of the Hall probe may have some errors, since the Bx and Bz component should be zero on the axis because of the symmetry, while the measured values have none zeros. According to the (Bx, By, Bz) values (15, -32, 1323) Gauss at the center, the rolling and the tilt angles are estimated as 0.65 degree and1.4 degree, respectively. The angle positioning of such a small device is not easy in the measurement.

5. Summary

We made a permanent magnet employing neodymium pieces to get better signal to noise ratio to find long-lived $\pi^+\pi^-$ atoms. The maximum magnetic field strength at the center was 1323 Gauss with the gap of 60 mm which was required by the beam halo interference to the magnet. The maximum field strength is within the allowed value not to quench the long-lived excited $\pi^+\pi^-$ atoms to the ground state. The magnetic field along the tracks is diminished enough at 10cm from the production target of Be, where the platinum foil is set not to bend the π^+ and π^- tracks after the break-up of the long-lived $\pi^+\pi^-$ atoms, while keeping the bending power BLy of 0.01T.m.

Although there are small differences between the simulated and the realized field strength,

the differences are not large problem in the bending function. The maximum field strength at the center and the bending power of BLy are consistent within 1.7 % and 0.02 %, respectively. In conclusion the magnet was fabricated to fulfill the requirements in Dirac experiment to find the long-lived $\pi^+\pi^-$ atoms.

Table 1: *Differences of BL between calculated data and experimental data.*

	BLx (mT.m) at x = y = 10 -100≦z≦0	BLx (mT.m) at x = y = 10 -100≦z≦100	BLz (mT.m) at x = y = 10 -100≦z≦0	BLy (T.m) at x = y = 0 -100≦z≦0	BLy (T.m) at x = y = 0 -100≦z≦100
Calculated Data	0.3052	0.6329	-1.2946	0.0047160	0.0097848
Experimental Data	0.3837	0.7536	-1.3397	0.0048083	0.0098021
Difference (%)	-27.4	-19.1	-3.5	-2.0	-0.2

	BLy (T.m) at x = y = 10 -100≦z≦0	BLy (T.m) at x = y = 10 -100≦z≦100	BLy (T.m) at x = y = -10 -100≦z≦0	BLy (T.m) at x = y = -10 -100≦z≦100
Calculated Data	0.00473365	0.00983605	0.00473365	0.00983605
Experimental Data	0.00489866	0.00986792	0.00477692	0.00987001
Difference (%)	-3.5	-0.3	-0.9	-0.3

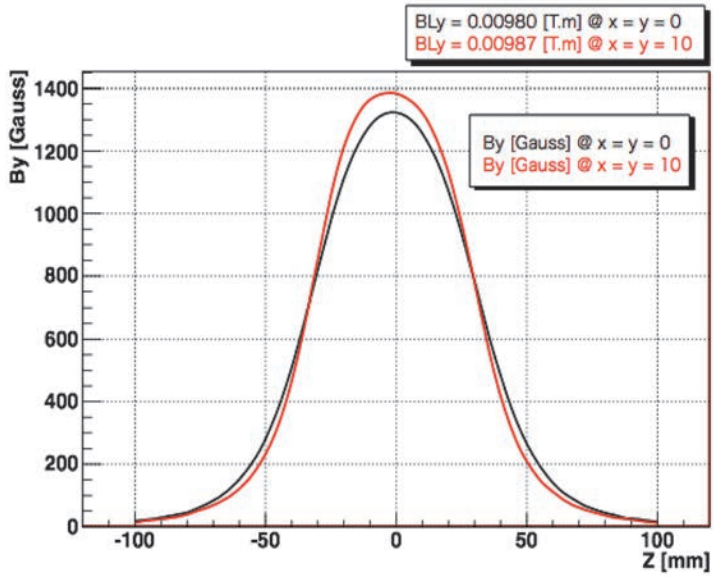

Fig. 13: *Graph of By at (x, y) = (0, 0) and (x, y) = (10, 10). The black line is at x = y = 0. The red line is at x = y= 10.*

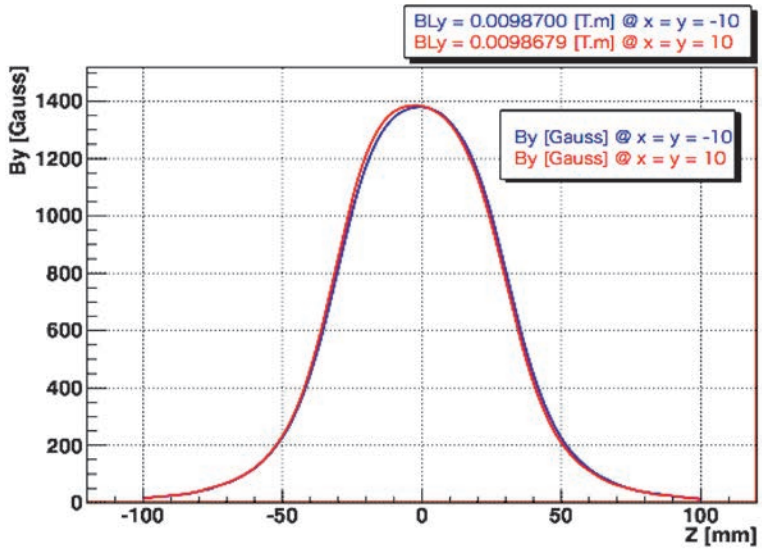

Fig. 14: *Graph of By at (x, y) = (-10, -10) and (x, y) = (10, 10). The blue line is at x = y = -10. The red line is at x = y = 10.*

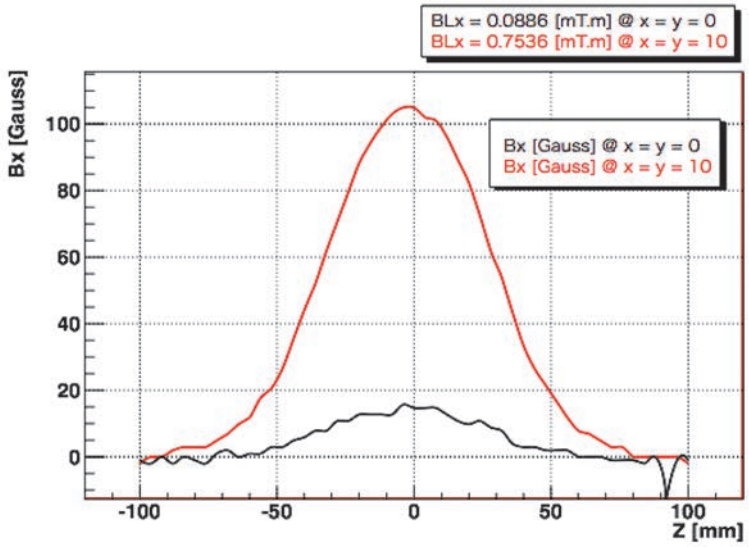

Fig. 15: *Graph of Bx at (x, y) = (0, 0) and (x, y) = (10, 10). The black line is at x = y = 0. The red line is at x = y = 10.*

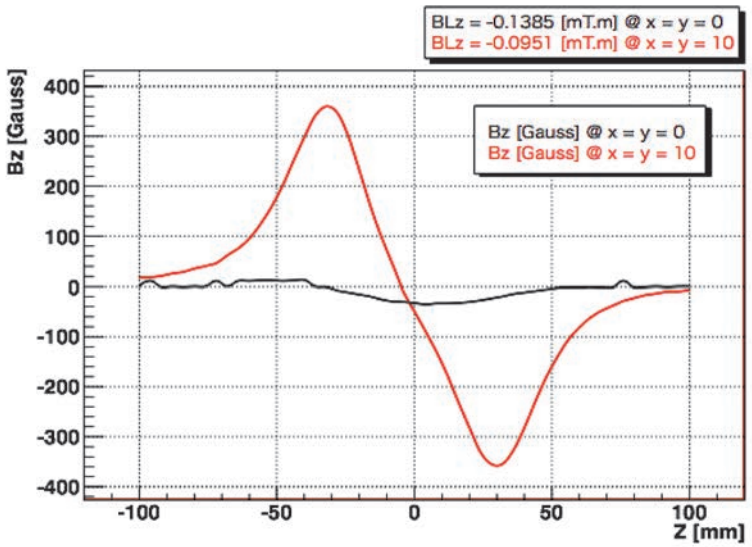

Fig. 16: *Graph of Bz at (x, y) = (0, 0) and (x, y) = (10, 10). The black line is at x = y = 0. The red line is at x = y = 10.*

References

[1] B. Adeva et al, Phys. Lett. B619(2005)50.

[2] B. Adeva et al, CERN-SPSC-2011-001/ SPSC-P-284 Add. 5 January 5, 2011.

[3] M.Chiba, A.Kuptsov and K.Okada, Dirac note 2001-06.

[4] A.Gorin et al., Nucl. Instr. & Meth. in Phys. Res. A566 (2006) 500.

[5] B.Adeva et al., Nucl. Instr. & Meth. in Phys. Res. A515 (2003) 467.

[6] O.-P. Kaehkoenen, S. Maekinen, M. Talvitie and M. Manninen: J. Phys.: Condens. Matter 4 (1992) p.1007-1014.

[7] T. Bizen, T. Tanaka Y. Asano, D. E. Kim, J. S. Bak, H. S. Lee and H. Kitamura: Nucl. Instr. & Meth. in Phys. Res. A467-468 (2001) p.185- 189.

[8] Yoshifumi Ito, Keisuke Yasuda, Ryoya Ishigami, Satoshi Hatori, Osami Okada, Ken Ohashi, and Shintaro Tanaka: Nucl. Instr. And Meth. in Phys. Res. B183 (2001) p.323- 328.

[9] P. Elleaume, O. Chubar, J. Chavanne, "Computing 3D Magnetic Field from Insertion Devices", Proc. of the PAC97 Conference, p.3509-3511.

[10] O. Chubar, P. Elleaume, J. Chavanne, "A 3D Magnetostatics Computer Code for Insertion devices", J. Synchrotron Rad. (1998) 5, p.481-484.

[11] O. Chubar, P. Elleaume, J. Chavanne, C. Benabderrahmane, O. Macouille, F. Marteau, "Application of Finite Volume Integral Approach to Computing of 3D Magnetic Fields Created by Distributed Iron-Dominated Electromagnet Structures", Proc. of the EPAC2004 Conference, p.1675-1677.

[12] http://www.senis.ch/3mh.html